Electronic Supplementary Material (ESI) for Physical Chemistry Chemical Physics.

Supporting Information

for

Study of the Exciton Dynamics in Perylene Bisimide (PBI) Aggregates with the Symmetrical Quasiclassical Dynamics based on the Meyer-Miller mapping Hamiltonian

Jie Zheng[1], Jiawei Peng[2,3], Yu Xie[2,3*], Yunze Long[1], Xin Ning[1], Zhenggang Lan[2,3*]

[1]Industrial Research Institute of Nonwovens & Technical Textiles, College of Textiles Clothing, Qingdao University, Qingdao 266071, China

[2]SCNU Environmental Research Institute, Guangdong Provincial Key Laboratory of Chemical Pollution and Environmental Safety & MOE Key Laboratory of Theoretical Chemistry of Environment, South China Normal University, Guangzhou 510006, China

[3]School of Environment, South China Normal University, University Town, Guangzhou 510006, China

Content

1. Frequencies and vibronic couplings

For the long-length PBI aggregates, the vibrational modes localized in each monomer unit displaying the large vibronic couplings are given in Table S1.

Table S1. Frequencies and vibronic couplings of the normal coordinates localized at each PBI monomer with $\kappa_j / \omega_j > 0.2$ and $\omega_j > 250$ cm^{-1}. [1]

ω_j /eV	κ_j /eV
0.0680	0.0266
0.0811	0.0194
0.1649	0.1120
0.1727	0.0720
0.1748	-0.0378
0.1823	-0.0383
0.1991	-0.1101
0.2020	-0.0642

2. Convergence of ML-MCTDH calculations

It is not trivial to make sure that convergence is achieved in the ML-MCTDH calculations. We have already discussed the general principles to construct the ML-MCTDH tree expansions and to get convergence calculations.[2-4] In practices, we set up an initial tree expansion and obtained the first result. Next, we modified the tree structure automatically by moving some branches from one node to another. The basis number of nodes in the bottom layer can be estimated according to the natural population of these nodes in calculation with the initial tree expansion. The nodes with similar basis number will be arranged in the same group in the new tree. Using this way, not the best but a reasonable tree can be obtained. At the same time, the number of basis in each layer was also increased. The next calculations were performed. The above procedure is repeated until the calculations are finally converged. We wrote the home-made programs to automatically generate tree structure, optimize the tree structure and increase the number of basis. In the current work, we first contrast a reasonable tree in the test calculations. Next we start to add more basis in this tree expansion (Figure S1), until the convergence of the ML-MCTDH calculations are reached.

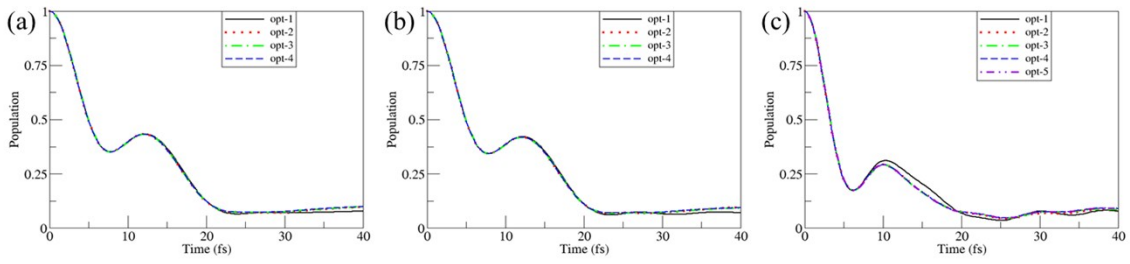

Figure S1. Population of the initial electronic state in the ML-MCTDH dynamics with the same tree structure and different basis numbers. Here opt-X (X is the repeated ML-MCTDH times) represents that the basis number is increased in each successive ML-MCTDH calculations. (a) The initial state is located at the first site in Model-I, (b) The initial state is located at first site in Model-II, (c) The initial state is located at the middle site in Model-II.

3. Exciton dynamics when the middle site of the one-dimensional PBI aggregate is excited

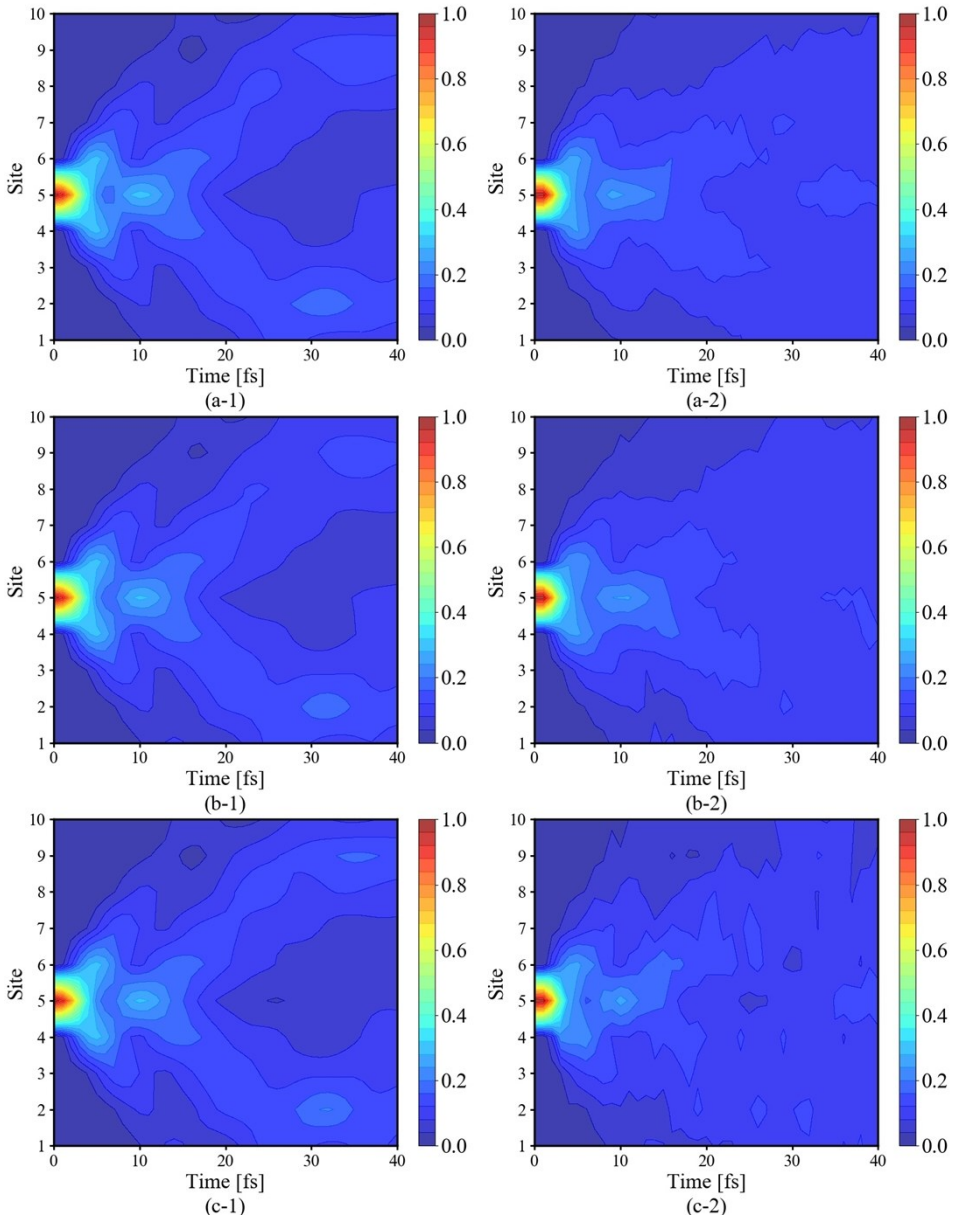

Figure S2. Exciton propagation in the 10-site PBI aggregate models using ML-MCTDH (labeled as '1') or SQC-MM (labeled as '2') methods when the middle site is excited. The labels of 'a', 'b' and 'c' correspond to the cases of Model-I, Model-II and Model-III.

4. Difference between ML-MCTDH and SQC-MM results

We plotted the ML-MCTDH and SQC-MM dynamics results of Model III with the initial state is located at the first site (Figure S3) and the middle site (Figure S4). It is reasonable to draw the conclusion that the SQC-MM method capture the main evolution feature of the ML-MCTDH dynamics, although the minor differences still exist. The SQC-MM method seems to slightly underestimate the population fluctuation over time for the sites far from the initial excited site.

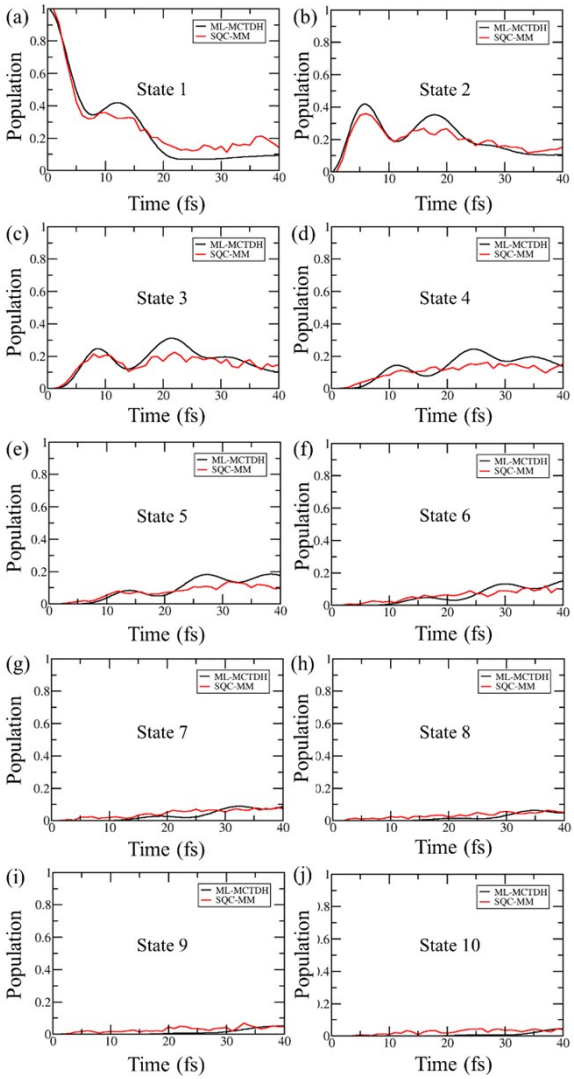

Figure S3. The time-dependent excited-state population at each site of Model III with initial state is located at first site, obtained with ML-MCTDH and SQC-MM dynamics.

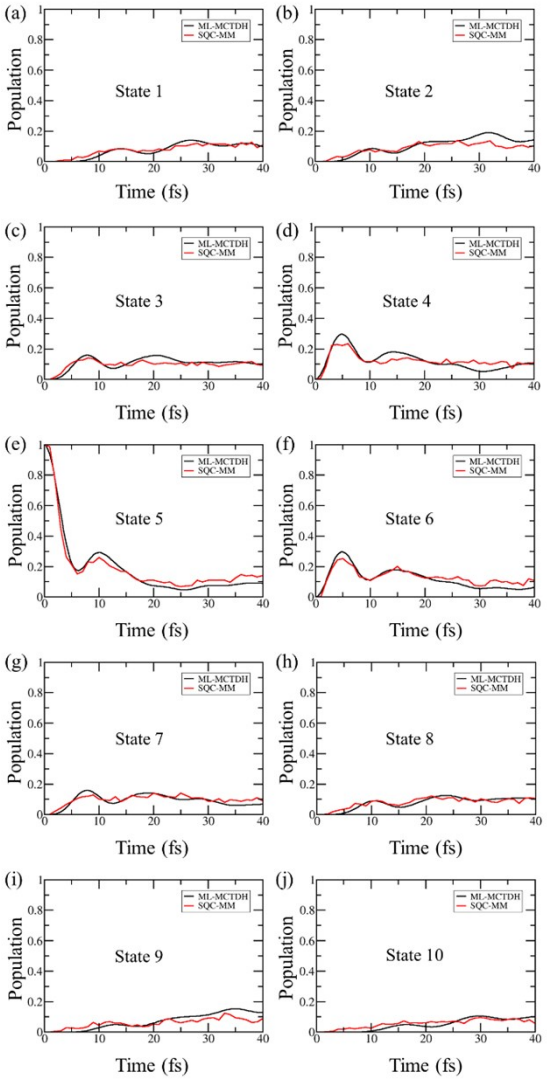

Figure S4. The time-dependent excited-state population at each site of Model III with the initial state is located at the fifth site, obtained with ML-MCTDH and SQC-MM dynamics.

5. Exciton diffusion for the short and long aggregates

The exciton dynamics with 61 and 101 sites based on the model with $V_c = 0.12$ eV are studied, which show minor different results, as shown in Figure S5.

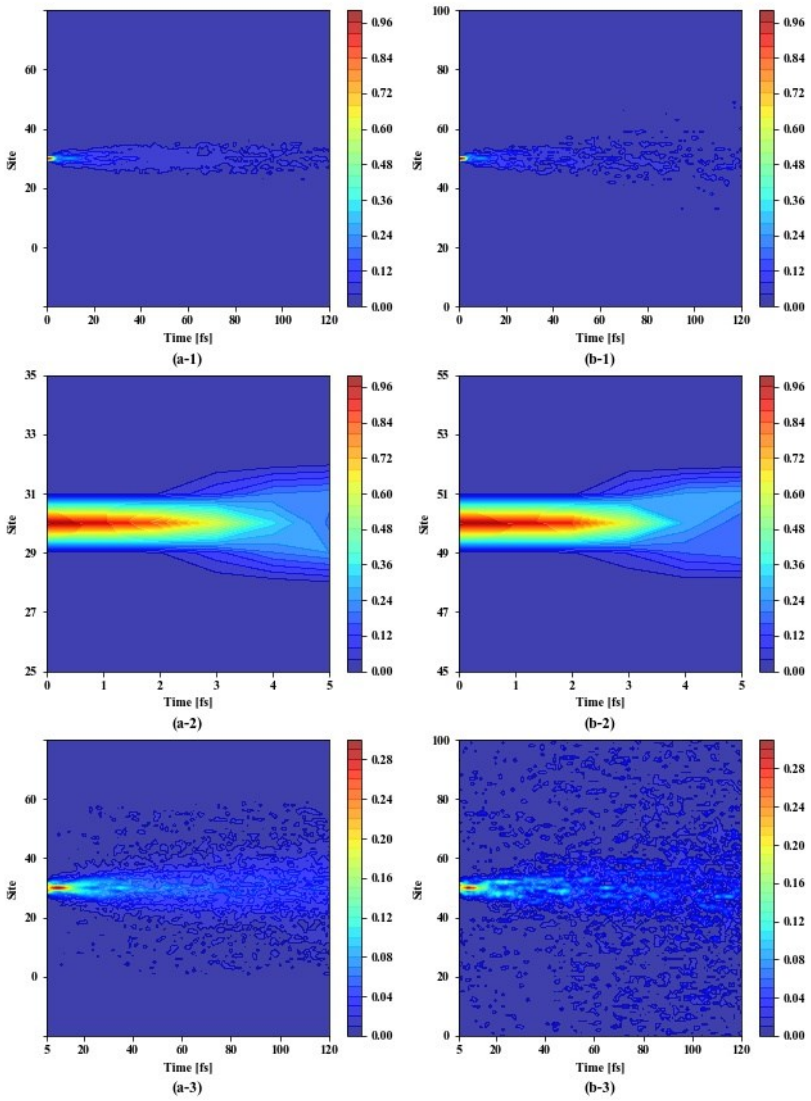

Figure S5. Exciton propagation in 61- (a) and 101-monomer (b) models (ω < 250 cm^{-1} and κ/ω > 0.2) using the SQC-MM method. Here the labels "1", "2" and "3" show the exciton dynamics of the whole propagation time (0-120 fs), the early time dynamics (0-5 fs) and the dynamics between 5 fs to 120 fs.

6. Snapshots of exciton density on exciton diffusion

The snapshots of the exciton density distribution of the long PBI aggregates with $V_c = \pm 0.05$ eV at different time are shown in Figure S6.

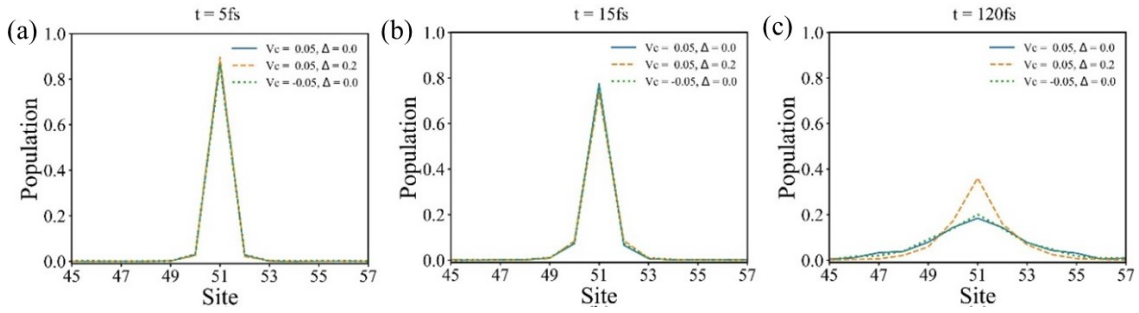

Figure S6. The the exciton density distribution of the 101-monomer models (ω < 250 cm^{-1}, κ/ω > 0.2, $V_c = \pm 0.05$ eV and with/without different static disorder) using the SQC-MM method. (a), (b) and (c) show the snapshots at 5, 15 and 120 fs.

Reference

1. Y. Xie, S. Jiang, J. Zheng and Z. Lan, *J. Phys. Chem. A*, 2017, **121**, 9567-9578.
2. S. Jiang, J. Zheng, Y. Yi, Y. Xie, F. Yuan and Z. Lan, *J. Phys. Chem. C*, 2017, **121**, 27263-27273.
3. J. Zheng, Y. Xie, S. Jiang and Z. Lan, *J. Phys. Chem. C*, 2016, **120**, 1375-1389.
4. Y. Xie, J. Zheng and Z. Lan, *J. Chem. Phys.*, 2015, **142**, 084706.